INTERFACE

royalsocietypublishing.org/journal/rsif

Research

Cite this article: Cam ME *et al*. 2020 Evaluation of burst release and sustained release of pioglitazone-loaded fibrous mats on diabetic wound healing: an *in vitro* and *in vivo* comparison study. *J. R. Soc. Interface* **17**: 20190712.
http://dx.doi.org/10.1098/rsif.2019.0712

Received: 13 October 2019
Accepted: 20 December 2019

Subject Category:
Life Sciences–Engineering interface

Subject Areas:
biomaterials, nanotechnology

Keywords:
burst release, sustained release, drug delivery, fibres, diabetic wound healing, pioglitazone

Authors for correspondence:
Muhammet Emin Cam
e-mail: m.cam@ucl.ac.uk
Mohan Edirisinghe
e-mail: m.edirisinghe@ucl.ac.uk

Electronic supplementary material is available online at https://doi.org/10.6084/m9.figshare.c.4798674.

THE ROYAL SOCIETY PUBLISHING

Evaluation of burst release and sustained release of pioglitazone-loaded fibrous mats on diabetic wound healing: an *in vitro* and *in vivo* comparison study

Muhammet Emin Cam[1,2,4], Sila Yildiz[5], Hussain Alenezi[1,6], Sumeyye Cesur[2,3], Gul Sinemcan Ozcan[7], Gokce Erdemir[8], Ursula Edirisinghe[9], Dilek Akakin[7], Durdane Serap Kuruca[10], Levent Kabasakal[4], Oguzhan Gunduz[2,3] and Mohan Edirisinghe[1]

[1]Department of Mechanical Engineering, University College London, Torrington Place, London WC1E 7JE, UK
[2]Center for Nanotechnology and Biomaterials Research, and [3]Department of Metallurgy and Material Engineering, Faculty of Technology, Marmara University, Istanbul 34722, Turkey
[4]Department of Pharmacology, Faculty of Pharmacy, Marmara University, Istanbul 34716, Turkey
[5]Centre for Discovery Brain Sciences, University of Edinburgh, George Square, Edinburgh EH8 9XD, UK
[6]Department of Manufacturing Engineering, College of Technological Studies, PAAET, 13092 Kuwait City, Kuwait
[7]Department of Histology and Embryology, Faculty of Medicine, Marmara University, Istanbul 34854, Turkey
[8]Department of Molecular Medicine, Aziz Sancar Institute of Experimental Medicine, Istanbul University, Istanbul 34093, Turkey
[9]Accident and Emergency Department, Hillingdon Hospital, NHS Foundation Trust, Pield Heath Road, Uxbridge UB8 3NN, UK
[10]Department of Physiology, Faculty of Medicine, Istanbul University, Istanbul 34093, Turkey

ME, 0000-0001-8258-7914

In order to provide more effective treatment strategies for the rapid healing of diabetic wounds, novel therapeutic approaches need to be developed. The therapeutic potential of peroxisome proliferator-activated receptor-γ (PPAR-γ) agonist pioglitazone hydrochloride (PHR) in two different release kinetic scenarios, burst release and sustained release, was investigated and compared with *in vitro* and *in vivo* tests as potential wound healing dressings. PHR-loaded fibrous mats were successfully fabricated using polyvinyl-pyrrolidone and polycaprolactone by scalable pressurized gyration. The results indicated that PHR-loaded fibrous mats expedited diabetic wound healing in type-1 diabetic rats and did not show any cytotoxic effect on NIH/3T3 (mouse embryo fibroblast) cells, albeit with different release kinetics and efficacies. The wound healing effects of fibrous mats are presented with histological and biochemical evaluations. PHR-loaded fibrous mats improved neutrophil infiltration, oedema, and inflammation and increased epidermal regeneration and fibroblast proliferation, but the formation of hair follicles and completely improved oedema were observed only in the sustained release form. Thus, topical administration of PPAR-γ agonist in sustained release form has high potential for the treatment of diabetic wounds in inflammatory and proliferative phases of healing with high bioavailability and fewer systemic side effects.

1. Background

Diabetes mellitus (DM) is a group of metabolic disorders, which occurs as a result of hyperglycaemia following insulin resistance and/or deficiency in insulin secretion [1]. Wounds associated with diabetes and poor healing are one of the most common serious complications, and may cause severe infections, potential amputation and poor quality of life [2]. Therefore, novel therapeutic approaches

need to be developed alongside the development of technology to regulate reactive oxygen species to improve the treatment of diabetic wounds.

In recent years, the study of controlled release of drugs and bioactive agents from polymeric materials has attracted the attention of many researchers from around the world [3]. Controlled drug delivery applications include both sustained delivery over days/weeks/months/years and targeted delivery on a single or sustained basis [4]. Controlled release formulations can be used to reduce the amount of drug necessary to provide the same therapeutic effect in patients. Another undoubted advantage is improved patient compliance. In many of the controlled release formulations, immediately upon placement in the release medium, an initial large bolus of drug is released before the release rate reaches a stable profile. This phenomenon is called 'burst release' and it leads to higher initial drug delivery and also reduces the effective lifetime of the device. Burst release has been used to deliver drugs at high release rates as part of the drug administration strategy [4,5]. Burst release may be the optimal mechanism of delivery in several instances. It has been shown that many drugs need to be administered at varying rates, and for some drugs, such as those used at the beginning of wound treatment, an initial burst provides immediate relief followed by prolonged release to promote gradual healing [6]. In order to ensure burst release, the matrix type (monolithic) controlled drug release system, which is a diffusion-controlled system, was created with polyvinylpyrrolidone (PVP) at three different polymer ratios. To compare burst release with sustained release, sustained release dosage form of pioglitazone hydrochloride (PHR) was successfully achieved using fibres blended with polycaprolactone (PCL). However, novel pressurized gyration (PG) was used to make the fibres (mats) [7,8].

PG process technique plays a crucial role in the mass production of fine fibres since it brings together controlled gas pressure and chamber rotation speed simultaneously [9]. The PG system consists of a rotary cribriform chamber which spins at 12 000–36 000 r.p.m. and 1×10^5–3×10^5 Pa of pressurized gas (nitrogen) applied inside the top of the chamber [10].

Peroxisome proliferator-activated receptors (PPARs) are ligand-activated transcription factors of the nuclear hormone receptor superfamily comprising the following three subtypes: PPAR-α, PPAR-γ and PPAR-β/δ. In skin wound healing, PPAR-α participates in the control of the early inflammation phase of the healing, PPAR-β regulates keratinocyte proliferation, adhesion and migration, and PPAR-δ promotes fibroblast proliferation. However, the role of PPAR-γ in wound healing is not well elucidated [11]. PPAR-γ has been studied especially in diabetes and obesity due to its role in regulating glucose metabolism, adipocyte differentiation and lipid metabolism. PPAR-γ has been recognized as playing a fundamentally important role in the immune response through its ability to inhibit the expression of inflammatory cytokines and to direct the differentiation of immune cells toward anti-inflammatory phenotypes [12]. It has been shown that PPAR-γ efficiency delays skin wound healing through impairing apoptotic cell clearance in mice [13]. Thus, it is theoretically possible that, in the future, tissue repair or fibrotic responses might be controlled by thiazolidinediones or similar drugs that modulate PPAR-γ activity. Synthetic PPAR-γ agonists such as thiazolidinediones (e.g. troglitazone, pioglitazone and rosiglitazone) are in clinical use to treat type 2 DM. In our study, PHR was chosen and loaded into PVP and PVP/PCL fibrous mats.

The novelty of this work is summarized as fibrous mats are used for the treatment of wound healing with two different release kinetics, burst release and sustained release. Both release kinetics are used as a treatment strategy for wound healing but there is no investigation for a comparison of these release kinetics in the same research with *in vivo* tests and further investigations with biochemical and histological analysis at specific time intervals. There is no literature on which release kinetics of drug-loaded fibrous mats will be more effective in which wound healing phase. However, there are a few reports investigating the *in vivo* biological outcomes of drug delivery systems with different release kinetic profiles. In this study, we examine the biological impact of different release kinetics of PHR-loaded fibres in a 14-day wound healing test in diabetic rats; also neutrophil infiltration, oedema, inflammation, epidermal regeneration and fibroblast proliferation were histologically and biochemically investigated at the wound site. Besides, morphology, physical and chemical composition, thermal properties, drug release behaviours, and *in vitro* cytotoxicity of PHR-loaded PVP fibres, PHR-loaded PVP/PCL fibres, and pure fibres were investigated.

2. Methods

Materials and methods for preparation and characterization of solutions, preparation and characterization of fibrous mats, scanning electron microscopy (SEM), attenuated total reflection-Fourier transform infrared spectroscopy (ATR-FTIR), X-ray powder diffraction (XRD), drug encapsulation efficiency, *in vitro* PHR release kinetic assay, tensile test of fibrous mats, methylthiazolydiphenyltetrazolium bromide (MTT) viability assay, *in vivo* wound healing experiments, biochemical analysis, histopathological analysis and statistical analysis are given in electronic supplementary material, information S1.

3. Results and discussion

3.1. Preparation of fibrous mats

Different solutions were prepared in order to fabricate fibrous mats using PG. Solution viscosity affects fibre size and morphology [14]. There is a direct correlation between viscosity and fibre quality. Also, the surface tension has a key role in influencing the PG process of polymer solutions. Fibres can be beaded or may not form due to high surface tension [15]. A lower surface tension promotes greater fibre stretching as less force is required to overcome the surface tension [16]. The surface tensions of pure PVP solutions were 11.5, 12.0, 12.9, 13.9 and 15.0 mN m^{-1} for 10%, 12%, 15%, 18% and 20% (w/v) PVP, respectively (figure 1*a*). At the same time, viscosities of pure PVP solutions were 231.6, 386.1, 830.0, 1158.0 and 2727.0 mPa s, respectively (figure 1*b*). By the adding PHR (12 mg ml^{-1}) to the solutions, surface tension and viscosity increased (12.1 versus 12.0 mN m^{-1} and 440.2 versus 386.1 mPa s for 12% (w/v) PVP solutions; 13.0 versus 12.9 mN m^{-1} and 894.5 versus 830.0 mPa s for 15% (w/v) PVP solutions; and 14.0 versus 13.9 mN m^{-1} and 1676.0 versus 1158.0 mPa s for 18% (w/v) PVP solutions, respectively). For pure PVP/PCL blended solutions, the surface tensions were measured as 14.7, 15.2 and 16.2 mN m^{-1}; and viscosities were measured as 610.4, 618.2 and 627.4 mPa s for the three different ratios ($w_{PVP}/w_{PCL} = 6/4$, 7/3 and 8/2,

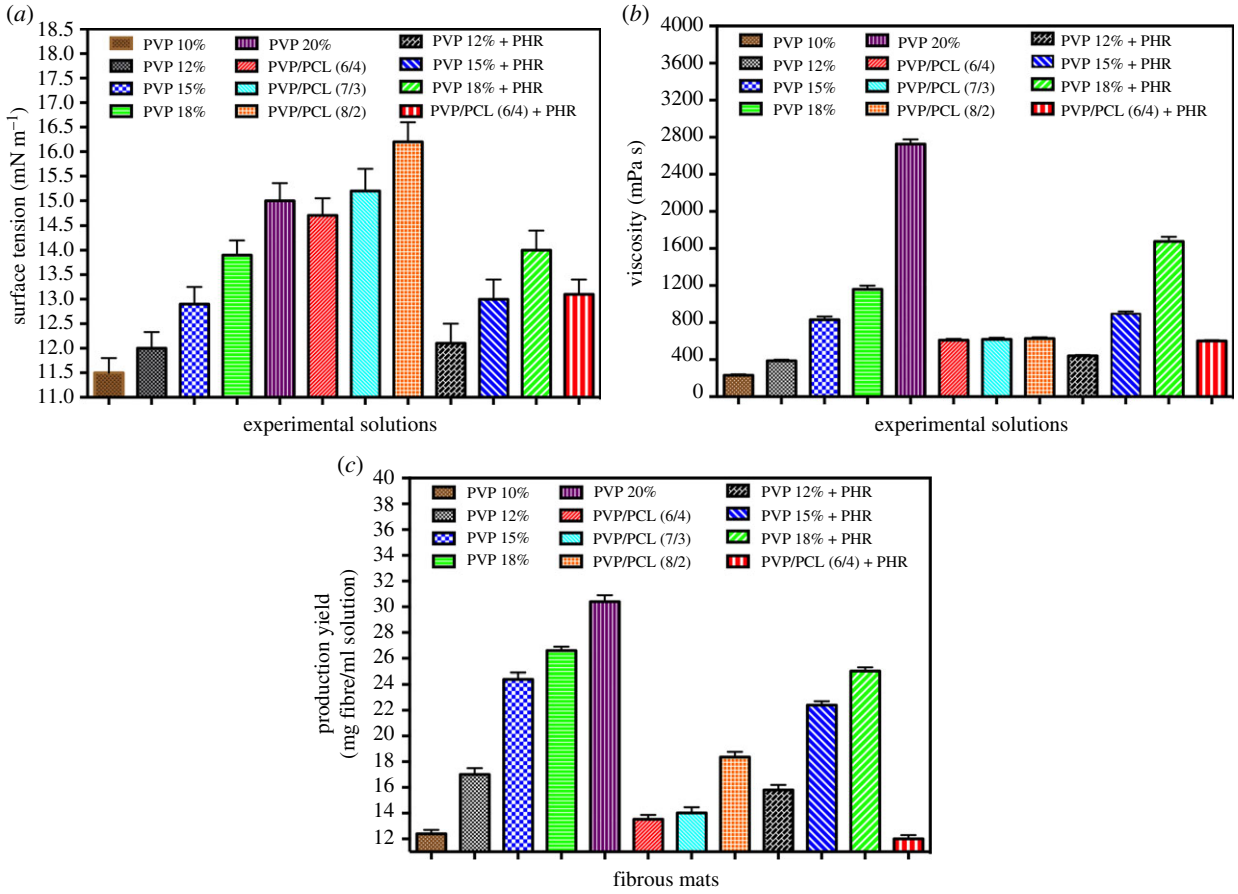

Figure 1. The key physical properties of all solutions used in the experiments: (*a*) surface tension and (*b*) viscosity. (*c*) The production yield of all fibrous mat samples. (Online version in colour.)

respectively). By adding PHR to the solution, surface tension and viscosity decreased (13.1 versus 14.7 mN m^{-1} and 601.0 versus 610.4 mPa s, respectively). All PHR solutions were tailored to have suitable properties and therefore bead-free fibrous mats were produced with 12%, 15% and 18% (w/v) PVP and 12% (w/v) PVP/PCL solutions.

In the PG process, there are several important parameters such as working pressure and rotational speed. The gas pressure affects the yield of fibres fabricated by PG. The production yields per millilitre for each sample were calculated (figure 1*c*). 36 000 r.p.m. and 1×10^5 Pa were chosen for the experiments. Ideal fibre morphologies and required production yield were not obtained at lower rotational speed and higher gas pressures.

3.2. Morphological characterization of fibrous mats

The change in the fibre size and morphology of pure PVP and PVP/PCL fibrous mats and also PHR-loaded PVP and PVP/PCL fibrous mats produced via PG in different polymer concentrations were investigated using SEM. Firstly, in order to determine the optimized PVP concentrations, pure fibrous mats in five different PVP concentrations (10%, 12%, 15%, 18%, 20%, w/v) were fabricated using PG. According to the results obtained, three different polymer ratios (12%, 15% and 18%, w/v) were chosen to fabricate PHR-loaded PVP fibres (figure 2).

Under the same PG conditions, fibres had greater diameter with increasing polymer concentration. At the lowest polymer concentration (10%, w/v), PVP fibres were of diameter $\varphi = 1512.62 \pm 455.02$ nm, and it increased to $\varphi = 1532.26 \pm 519.19$, $\varphi = 1539.47 \pm 677.15$, $\varphi = 2031.96 \pm 893.54$ and $\varphi = 3216.92 \pm 1699.42$ nm for 12%, 15%, 18% and 20% (w/v), respectively (electronic supplementary material, figure S1). Although the lowest fibre diameter belongs to 10% PVP fibres, the lowest frequency (approx. 20%) and the lowest production yield (12.4 mg ml^{-1}) were also obtained at that ratio. Besides, 12% PVP fibres had similar diameter but the production yield (17 mg ml^{-1}) was higher than 10% PVP fibres. Therefore, 10% PVP concentration was not preferred for further studies. On the other hand, 20% PVP concentration was not chosen due to larger diameter fibres and beaded morphology, compared to other ratios. The production yields of pure PVP fibres from the lowest concentration to highest were 12.4, 17.0, 24.4, 26.6 and 30.4 mg ml^{-1} solution, respectively.

When we examine the PHR-loaded PVP fibres, production of those fibres with 12%, 15% and 18% PVP solutions caused fibres to be homogeneously dispersed and distributed within the polymer matrices. The diameter of fibres decreased considerably by adding PHR compared to their pure forms. The diameters of PHR-loaded 12%, 15% and 18% PVP fibres were $\varphi = 603.24 \pm 163.50$, $\varphi = 1093.47 \pm 335.98$ and $\varphi = 1118.10 \pm 454.44$ nm, respectively (electronic supplementary material, figure S1). However, the production yields of PHR-loaded fibrous mats were lower than pure PVP fibrous mats in the same polymer ratios: 15.8, 22.4 and 25.0 mg ml^{-1} solution at 12%, 15% and 18% polymer ratios, respectively.

The same strategy was pursued to determine the optimized PVP/PCL ratios and pure fibrous mats of the three different PVP/PCL concentrations ($w_{PVP}/w_{PCL} = 6/4$, 7/3 and 8/2; 12%, w/v) were fabricated using PG. According to the results obtained, PHR-loaded PVP/PCL fibre was fabricated with

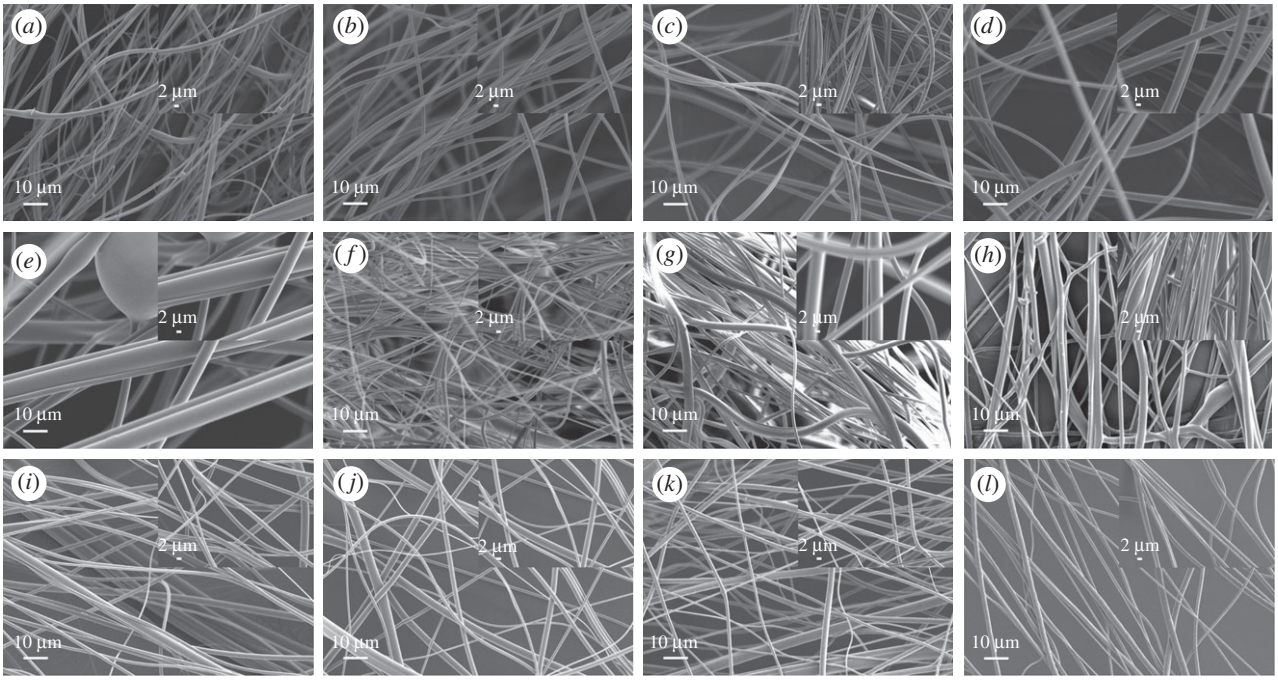

Figure 2. SEM images of pure PVP fibrous mats and PHR-loaded PVP fibrous mats: (*a*) 10% (w/v) PVP, (*b*) 12% PVP, (*c*) 15% PVP, (*d*) 18% PVP, (*e*) 20% PVP, (*f*) PHR-loaded 12% PVP, (*g*) PHR-loaded 15% PVP, (*h*) PHR-loaded 18% PVP fibrous mats. SEM images of pure PVP/PCL (12%, w/v) fibrous mats and PHR-loaded PVP/PCL (12%, w/v) fibrous mats: (*i*) $w_{PVP}/w_{PCL} = 8/2$ PVP/PCL, (*j*) $w_{PVP}/w_{PCL} = 7/3$ PVP/PCL, (*k*) $w_{PVP}/w_{PCL} = 6/4$ PVP/PCL, (*l*) PHR-loaded ($w_{PVP}/w_{PCL} = 6/4$) PVP/PCL fibrous mats.

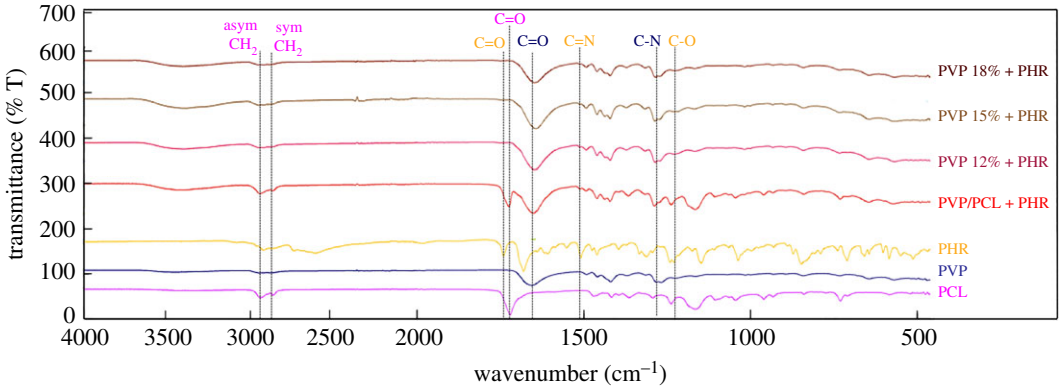

Figure 3. FTIR spectra of pure PCL, pure PVP, pure PHR, PHR-loaded PVP fibrous mats at three different concentrations (12%, 15% and 18%), and PHR-loaded PVP/PCL fibrous mats. (Online version in colour.)

the optimized polymer ratio ($w_{PVP}/w_{PCL} = 6/4$, 12%, w/v) (figure 2). It was observed that the diameter of fibres increased with the increase of PCL ratio in PVP/PCL fibrous mats. The diameter of fibres for pure PVP/PCL ($w_{PVP}/w_{PCL} = 8/2$) fibres was $\varphi = 677.40 \pm 230.89$ nm and it increased to $\varphi = 805.62 \pm 350.98$ and $\varphi = 812.17 \pm 345.36$ nm at $w_{PVP}/w_{PCL} = 7/3$ and $w_{PVP}/w_{PCL} = 6/4$ polymer ratios, respectively (electronic supplementary material, figure S2).

The fibre diameter is one of the variables that can be controlled to arrange the rate of fibre dissolution and alter drug release. In brief, fibre of higher diameter has lower surface area and would lead to a delayed release compared to smaller diameter fibre. In this study, since we have focused on drug release differences and we aim to reveal these differences in the clearest way, fibre with the highest PCL ratio ($w_{PVP}/w_{PCL} = 6/4$) was chosen to load PHR for further studies. Furthermore, the fact that its homogeneity was quite similar to the other two fibre ratios was another advantage that led to the selection of ratio ($w_{PVP}/w_{PCL} = 6/4$). The production yields of pure PVP/PCL fibres were 13.52, 14.00 and 18.36 mg ml^{-1} solution for $w_{PVP}/w_{PCL} = 6/4$, 7/3 and 8/2, respectively. The diameter of fibres increased due to adding PHR ($\varphi = 900.67 \pm 390.98$) compared to the pure form (electronic supplementary material, figure S2). Additionally, the production yield of PHR-loaded fibrous mats (12.00 mg ml^{-1}) was lower than pure PVP fibrous mats.

3.3. Fibre composition

ATR-FTIR was used to analyse molecular contents of fibrous mats and it was confirmed that PHR was encapsulated successfully into the PVP and PVP/PCL fibrous mats. The molecular structures of pure PVP, pure PCL, pure PHR and all PHR-loaded fibrous mats fabricated by PG are shown in figure 3 and spectra of pure fibrous mats are given in electronic supplementary material, figure S3, which shows the characteristic C=O stretching peak for the crystalline component at 1720 cm^{-1}, CH_2 asymmetric and symmetric stretching bands at 2945

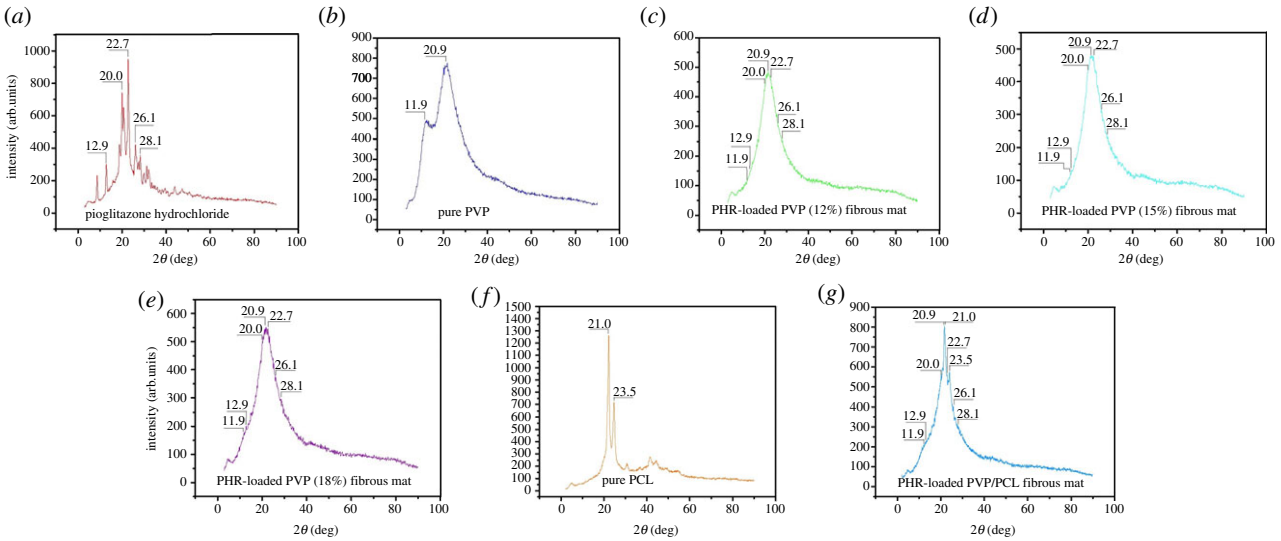

Figure 4. XRD patterns of (*a*) PHR powder, (*b*) pure PVP, (*c*) PHR-loaded PVP (12%) fibrous mat, (*d*) PHR-loaded PVP (15%) fibrous mat, (*e*) PHR-loaded PVP (18%) fibrous mat, (*f*) pure PCL and (*g*) PHR-loaded PVP/PCL fibrous mat. (Online version in colour.)

and 2866 cm^{-1}, respectively; C–H group bending at 1471 and 1417 cm^{-1}, O–H bending at 1396 and 1364 cm^{-1}; C–O stretching band in the crystalline phase at 1293 cm^{-1}, C–O–C asymmetric and symmetric stretching bands at 1238 and 1165 cm^{-1} all belong to PCL. The latter is the amorphous phase of PCL. For pure PVP, the O–H stretching vibration band at 3439 cm^{-1} is caused by amide–iminol tautomerism, C–H asymmetric stretching band at 2944 cm^{-1}, characteristic amide C=O stretching vibration, the most intensive absorption band, at 1655 cm^{-1} are found. CH_2 scissoring at 1492 cm^{-1}, C–N stretching vibrations at 1459 and 1419 cm^{-1}, C–H bending bands at 1371 and 1314 cm^{-1}, the characteristic absorption bands of C–N stretching at 1282 and 1268 cm^{-1}, and CH_2 twist bands at 1226 and 1166 cm^{-1} are also observed [7,8].

FTIR spectra of PHR pure drug shows peaks at 2925 and 2740 cm^{-1} due to aliphatic C–H asymmetric and symmetric stretching [17]. The characteristic bands are amide C=O stretching at 1741 cm^{-1}, C=N stretching at 1509 cm^{-1} and C–O stretching at 1242 cm^{-1}. Besides, C=C stretching at 1607 cm^{-1}, ring C–N stretching at 1461 cm^{-1}, aliphatic C–O–C at 1109 cm^{-1} and C–S stretching at 659 cm^{-1} were observed [18]. Compared with the pure PVP and PCL absorption spectra, new peaks at 1741, 1509 and 1242 cm^{-1} belonging to PHR were observed in all PHR-loaded fibrous mats. For the PCL/PVP composite system, peaks at 2945, 2866 and 1720 cm^{-1} belong to PCL and the peaks at 1655 and 1282 cm^{-1} belong to PVP. These results indicate successful formulation and drug encapsulation. Besides, it was observed that there was no polymer–drug interaction.

3.4. X-ray powder diffraction

XRD studies were carried out on all PHR-loaded samples to confirm the encapsulated PHR in the PVP and PVP/PCL fibrous mats and pure samples to confirm accurate production (figure 4 and electronic supplementary material, figure S4, respectively). The XRD pattern of PHR is characterized by major peaks at 12.9, 20.0, 22.7, 26.1 and 28.1 2θ. The diffraction peaks of PVP were found at 11.9 and 20.9 2θ [19,20]. XRD results confirm that existing compounds were found in PHR-loaded PVP fibrous mats. PCL is characterized by a sharp peak at 21.0 2θ and a relatively low-intensity peak at 23.5 2θ and these peaks show the crystalline nature of PCL in pure and PHR-loaded PVP/PCL fibrous mats [21]. The halo diffraction pattern sighted between 10 and 40 2θ is the characteristic amorphous material showing a degree of amorphous characteristic in the drug-loaded fibrous mats, which is most probably related to the polymeric carrier [22].

3.5. Tensile properties of fibrous mats

Tensile strength and strain at break are shown in figure 5*a*,*b*, respectively. These results show that pure fibrous mats have greater tensile strength than PHR-loaded fibrous mats at the same polymer ratios (0.274 ± 0.114 versus 0.244 ± 0.146 MPa for PVP 12%; 0.796 ± 0.277 versus 0.274 ± 0.220 MPa for PVP 15%; 0.805 ± 0.287 versus 0.389 ± 0.212 MPa for PVP 18%; 0.677 ± 0.253 versus 0.321 ± 0.105 for PVP/PCL 12%). Besides, PVP/PCL composite fibres have better tensile strength compared to PVP fibres in the same polymer ratio (12%, w/v). We observed similar outputs from the results of strain at break. It is clearly seen that the tensile strength increases as the fibre diameter increases.

3.6. Melting behaviour of fibrous mats

The melting temperatures (Tm) of the PVP/PCL composites were close to the value of 60°C normally found for pure PCL. The Tm of pure PVP/PCL and PHR-loaded PVP/PCL fibrous mats were 61.45°C and 60.95°C, respectively. The addition of PHR to the polymer composite slightly decreased the Tm. The Tm could not be seen in PVP samples due to the amorphous structure (electronic supplementary material, figure S5).

3.7. *In vitro* drug release

In vitro drug release kinetic assays for PHR-loaded fibrous mats were performed according to the first-order model. Primarily, the UV spectra were obtained with the concentration range of PHR from 2 to 10 µg ml^{-1} and a linear standard calibration curve was drawn from PHR absorption values (R^2 = 0.99925) obtained for the quantitative determination of drug release (figure 6*a*). The released PHR was determined from UV absorbance measured at 216 nm. Besides, the encapsulation efficiencies within the PHR-loaded fibres were calculated and they are relatively high (figure 6*b*). The highest

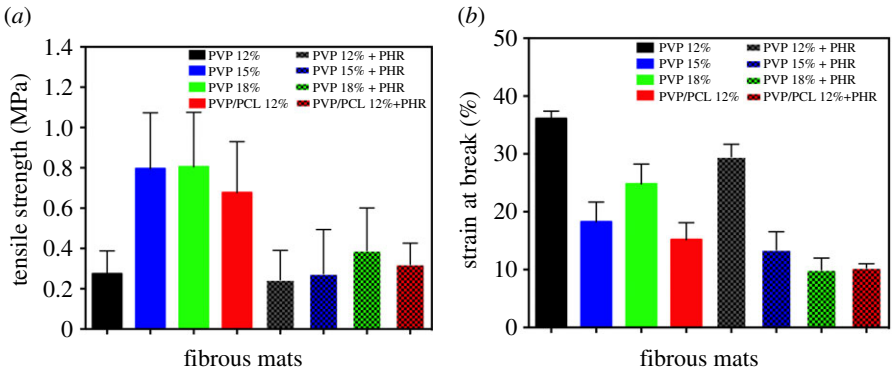

Figure 5. Physical parameters of fibrous mats: (*a*) tensile strength and (*b*) strain at break. PVP 12%: pure PVP (12%) fibrous mat; PVP 15%: pure PVP (15%) fibrous mat; PVP 18%: pure PVP (18%) fibrous mat; PVP/PCL 12%: pure PVP/PCL (12%) fibrous mat; PVP 12% + PHR: PHR-loaded PVP (12%) fibrous mat; PVP 15% + PHR: PHR-loaded PVP (15%) fibrous mat; PVP 18% + PHR: PHR-loaded PVP (18%) fibrous mat; PVP/PCL 12% + PHR: PHR-loaded PVP/PCL (12%) fibrous mat. (Online version in colour.)

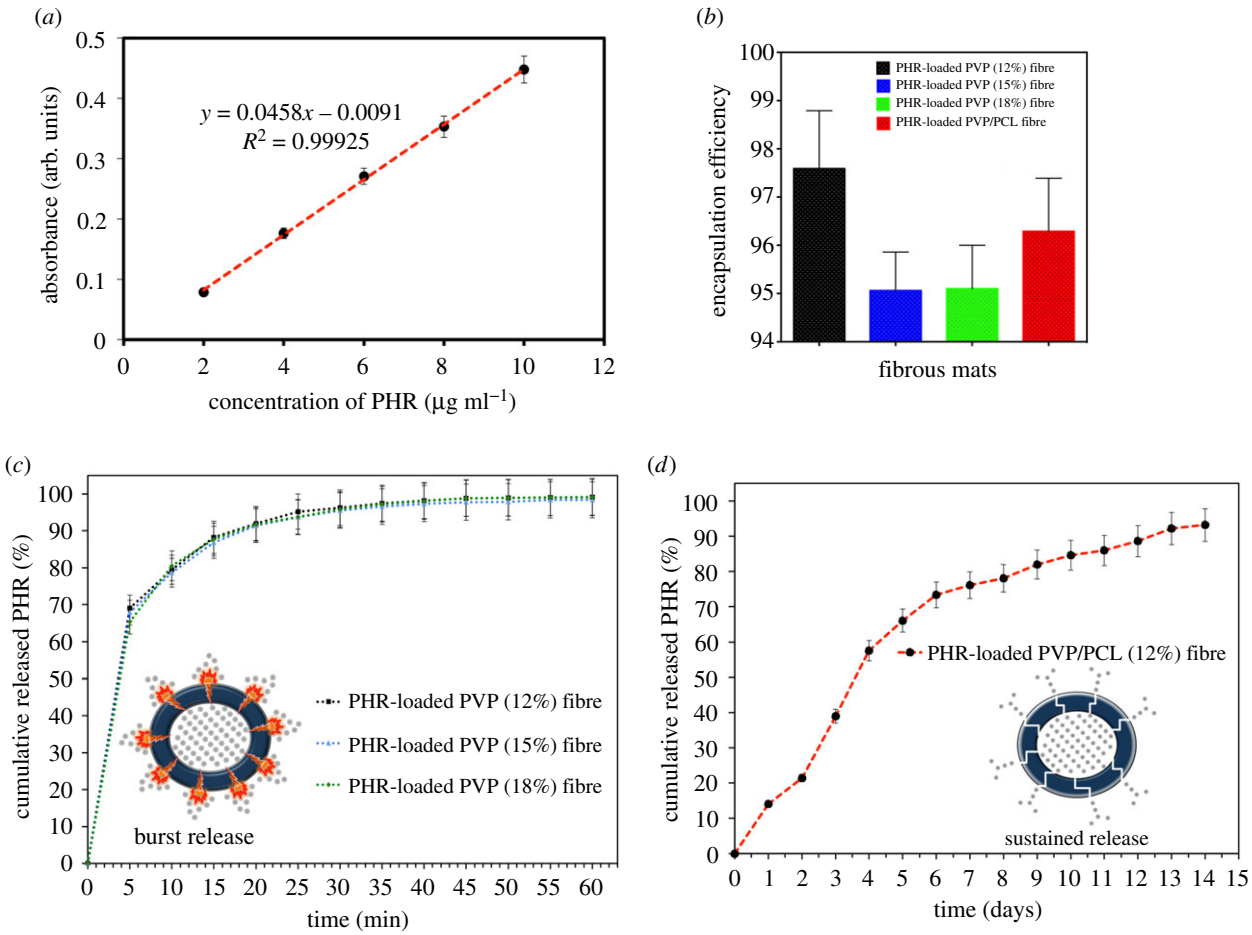

Figure 6. *In vitro* drug release profiles of fibrous mats: (*a*) PHR calibration curve, (*b*) encapsulation efficiencies of PHR-loaded fibres, (*c*) PHR release profiles at three different PVP ratios (12%, 15% and 18%, w/v) and (*d*) PHR release profile of PHR-loaded PVP/PCL (12%, w/v) fibres according to first-order model. All the values were obtained from the averages of three experiments, and the errors were less than 5%. (Online version in colour.)

encapsulation efficiency for PHR-loaded fibres belongs to PHR-loaded PVP (12%) with 97.59 ± 1.23%. Afterwards, *in vitro* release studies were performed over a period of 14 days for PHR-loaded PVP/PCL fibres and for 1 h for PHR-loaded PVP fibres in order to determine the release kinetics of encapsulated PHR. The release profiles of PHR-loaded fibres were measured in phosphate-buffered saline of pH 7.4 and a controlled temperature of 37°C to mimic the physiological conditions of living organisms.

As shown in figure 6*c*, all of the PHR-loaded PVP fibres showed a burst drug release in approximately 60 min, which is attributed to the highly water soluble nature of PVP. However, PHR release rates were different for various polymer ratios. PHR release rate reached 69.1% in PVP (12%) fibres, while drug release from the two other fibres reached 67.8% and 65.3% for PVP (15%) and PVP (18%) ratios, respectively. When the polymer ratio increased in PHR-loaded PVP fibres from 12% to 18%, the released PHR ratio in the first 5 min decreased from 69.1% to 65.3%.

On the contrary, PHR-loaded PVP/PCL fibres showed a sustained drug release over 14 days, which is attributed to the hydrophobic character of PCL (figure 6*d*). PHR was

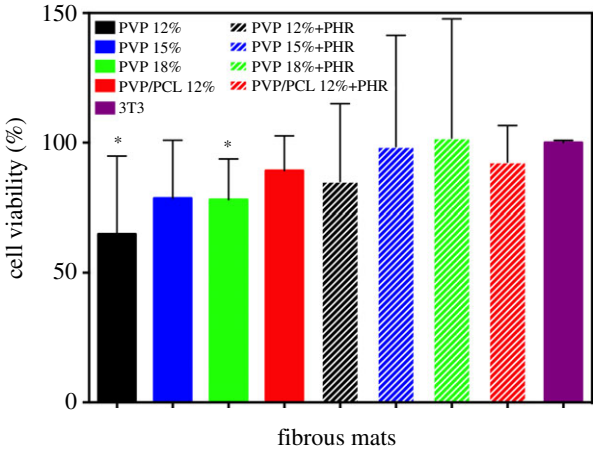

Figure 7. NIH/3T3 (mouse embryo fibroblast) cell viability of pure and PHR-loaded fibrous mats at the end of 72 h. The data are presented as mean ± s.e.m. *$p < 0.05$ versus control group (3T3). (Online version in colour.)

released in a controlled manner until the last day of the test and peaked on 14th day. In total, 93% of encapsulated PHR was released within 14 days for PVP/PCL fibre. As a result, PHR was released from PVP and PVP/PCL fibres successfully but PVP/PCL fibres demonstrated a much slower rate compared to PVP fibres. Besides, the biological effects of different drug release kinetics for PHR were observed in diabetic wound healing in rats.

3.8. Evaluation of cell viability

The cytotoxicity of the fibrous mats was evaluated by the MTT assay. The cytotoxicity test indicated that PHR-loaded fibrous mats had no cytotoxic effect compared to control at 72 h (figure 7). In pure fibrous mats, only two different concentrations (12% and 18%, w/v) of PVP fibres showed cytotoxic effects ($p < 0.05$) compared to control group (3T3). Therefore, these PVP fibres were not applied as a control group in animal trials. As a result, the biocompatibility test demonstrated that PHR-loaded fibrous mats have suitable cytocompatibility, and can be recommended for the further development of biomedical applications.

3.9. Evaluation of wound healing ability

The *in vivo* tests consist of four different groups. The experimental design of wound healing experiments is shown in detail in electronic supplementary material, figure S6. PVP/PCL (12%, w/v) fibres were chosen as the pure fibre group because they did not show any cytotoxic effects compared to pure PVP fibres and also PHR-loaded PVP (12%, w/v) fibres were chosen for burst release investigations because they had better morphology and smaller diameter compared to the other PHR-loaded PVP fibres. Wound areas of diabetic animals were monitored during the healing process. Representative illustrations from an animal belonging to each group (control, pure PVP/PCL fibres, PHR-loaded PVP fibres, PHR-loaded PVP/PCL fibres) on days 0, 3, 7, 14 following wound creation are given in figure 8*a*. Although there were no significant macroscopic alterations on the first 3 days, wound closures in C and D groups on 7th day were visibly faster than those in A and B groups. Especially, it can be clearly observed that D group displayed a faster healing process on day 7. The changes in the wound areas on several days reflect different parts of the healing process (figure 8*b*).

On day 3, the animals treated with both PHR-loaded PVP ($p < 0.01$) and PVP/PCL fibres ($p < 0.001$) showed a significant fall in wound area compared to those in control and pure PVP/PCL groups. Thus, the means of the wounded area with PHR-loaded PVP and PHR-loaded PVP/PCL fibres decreased to 66.3 ± 5.1% and 69.7 ± 3.8%, respectively, when control animals decreased to 82.5 ± 4.9%. PHR-loaded PVP fibre group showed a better improvement ($p < 0.05$) in wound closure than PHR-loaded PVP/PCL fibre group on day 3. This reversion could be attributed to burst release of PHR from PVP fibres on day 3 because it provides more PHR concentration in the wound environment compared with PVP/PCL fibres. Conversely, on day 7, animals treated with PHR-loaded PVP/PCL fibres displayed a better recovery ($p < 0.05$) than those with PHR-loaded PVP fibres. It can be said that for day 7, due to the decrease in the amount of PHR release from PVP fibre, the healing effect was less. However, the sustained release of PHR from PVP/PCL fibres probably provided a more effective drug concentration than those affected by burst release in the wound area on day 7. Hence, the curative effect of burst release was inferior to those of sustained release at this time point. After that, there is no significant difference between PHR-loaded fibre groups on days 10, 12 and 14.

When we consider the 12th and 14th day, there is no significant difference in wound closure among treatment groups; considered to be the normal wound healing process. Besides, no remarkable differences were observed between groups macroscopically in figure 8*a*. Although animals with pure PVP/PCL fibres healed faster than control animals, they showed slower wound healing than PHR-loaded fibres at each time point except on days 12 and 14. These results are consistent with our previous estimations about diabetic wound healing, which are the burst release of PHR from PVP fibre, reaching high concentration and showing a better prognosis than other fibre groups did on day 3. Then, on day 7, PHR-loaded PVP/PCL fibre groups showed significant improvement in wound closure compared to PHR-loaded PVP fibre groups due to the sustained release of PHR.

Wound healing is a process that includes four stages occurring in synchrony, namely haemostasis, inflammation, proliferation and remodelling. Broadly, the inflammatory phase lasts around 6 days following an injury and several leucocytes like macrophages migrate into the wound area. The proliferative phase involves the proliferation of fibroblasts and keratinocytes and happens between days 4 and 10 following wound creation. The fourth phase, remodelling, begins around day 7. During this phase, the formation of extracellular matrix and collagen fibres increases. In diabetes, the healing process is not well orchestrated due to excessive inflammatory reactions so chronic ulcerations develop. As a PPAR-γ agonist, PHR shows potential anti-inflammatory properties. In some studies, it is claimed that PPAR-γ plays a key role in suppressing the fibrogenic response by antagonizing TGF-β activity on wound healing [23]. In this study, we ascertained this claim to be the opposite and we observed that PHR led to a faster wound healing in diabetic conditions. It is also found that the healing effect of PHR began from day 3 and lasted to day 14. The beneficial effects of PHR on days 3 and 10 were stronger than those of other days. Hence, we hypothesize that PHR has curative properties in diabetic wound healing especially for inflammatory and proliferative phases, and these effects come from its anti-inflammatory actions.

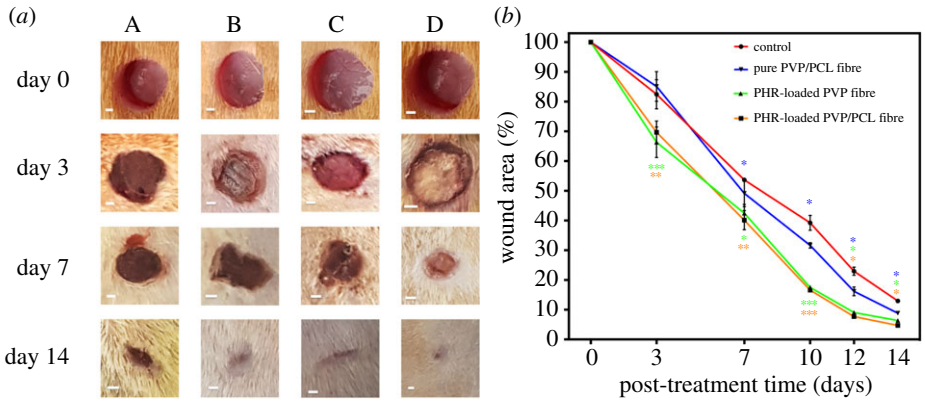

Figure 8. (*a*) Appearance of healing wound on days 0, 3, 7 and 14 after surgical incision: (A) control group, (B) pure PVP/PCL fibre group, (C) PHR-loaded PVP (12%) fibre group and (D) PHR-loaded PVP/PCL (12%) fibre group (scale bar = 1 mm). (*b*) Change in wound area after various treatments. The data are presented as mean ± s.e.m. Values are represented statistically when $*p < 0.05$, $**p < 0.01$, $***p < 0.001$ in comparison with control group. PVP 12%: pure PVP (12%) fibrous mat; PVP 15%: pure PVP (15%) fibrous mat; PVP 18%: pure PVP (18%) fibrous mat; PVP/PCL 12%: pure PVP/PCL (12%) fibrous mat; PVP 12% + PHR: PHR-loaded PVP (12%) fibrous mat; PVP 15% + PHR: PHR-loaded PVP (15%) fibrous mat; PVP 18% + PHR: PHR-loaded PVP (18%) fibrous mat; PVP/PCL 12% + PHR: PHR-loaded PVP/PCL (12%) fibrous mat. (Online version in colour.)

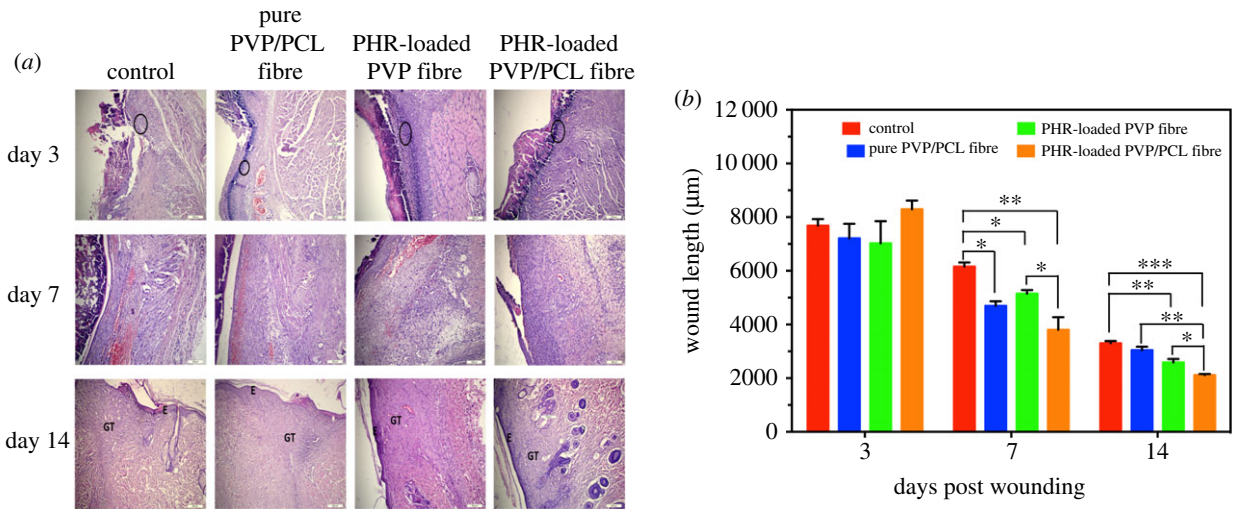

Figure 9. Histopathological evaluations. (*a*) Representative microscopic images of wounds from control, pure PVP/PCL fibre, PHR-loaded PVP fibre and PHR-loaded PVP/PCL fibre groups on days 3, 7 and 14. The circles indicate neutrophil infiltration. GT, granulation tissue; E, epithelium. Haematoxylin and eosin staining. Scale bars: 200 µm. (*b*) Comparison of wound length between all groups on days 3, 7 and 14. The values were calculated as the mean ± s.e.m. ($n = 6$), $***p < 0.001$, $**p < 0.01$, $*p < 0.05$. The statistical analyses were carried out with ANOVA test with Bonferroni's *post hoc* test. (Online version in colour.)

3.10. Evaluation of histological outcomes

The wounded tissues were stained with haematoxylin and eosin (H&E), and their histopathology was investigated and scored on days 3, 7 and 14 (figure 9 and table 1). Histological images of skin wounds from each of the four groups are shown in figure 9*a*. On day 3, neutrophil infiltration and oedema were evident in all groups with scab formation and few disorganized collagen fibres and fibroblasts. Besides, decreased neutrophil infiltration was observed only in PHR-loaded PVP fibres due to burst release kinetics of PHR. On day 7, decreased oedema and neutrophil infiltration, and increased epidermal regeneration and fibroblast proliferation in both PHR-loaded fibre groups were observed compared to the other groups. However, PHR-loaded PVP/PCL fibres showed stronger effects on decreasing oedema and neutrophil infiltration, and increasing epidermal regeneration. On day 14, PHR-loaded fibre groups showed clearly developed epithelialization, and increased fibroblast proliferation compared to the other groups. No neutrophil infiltration was observed in both PHR-loaded fibre groups but oedema was improved completely only in PHR-loaded PVP/PCL group (table 1). In addition to this, the formation of hair follicles was observed only in the PHR-loaded PVP/PCL fibre groups. Wound length measurements were made in rats of all four groups (figure 9*b*). On day 3, no significant difference between groups was observed; however, on days 7 and 14, both PHR-loaded PVP and PHR-loaded PVP/PCL fibre groups revealed decreased wound length ($p < 0.05$) in comparison to controls. The PHR-loaded PVP/PCL fibre group had significantly lower wound length compared to the PHR-loaded PVP fibre group on both days 7 and 14 ($p < 0.05$). The indexes mentioned in electronic supplementary material, table S1, were used for the scoring.

3.11. Evaluation of biochemical analysis

The concentration of a pro-inflammatory cytokine, TNF-α, in the wound areas on day 14 was measured according to the manufacturer's instruction using an ELISA kit (figure 10). On the last day of the experiment the expression level of TNF-α was significantly lower in PHR-loaded PVP fibres

Table 1. Histological scoring on days 3, 7 and 14. H&E stained sections ($n = 6$ in each group) were scored as none (−), mild (+), moderate (++) and severe (+++).

	epidermal regeneration	fibroblast proliferation	neutrophils	oedema
(*a*) day 3				
control	−	−	+++	+++
pure PVP/PCL fibres	−	−	+++	+++
PHR-loaded PVP fibres	−	−	++	++
PHR-loaded PVP/PCL fibres	+	−	+++	++
(*b*) day 7				
control	+	+	++	+++
pure PVP/PCL fibres	+	+	++	++
PHR-loaded PVP fibres	+	++	++	++
PHR-loaded PVP/PCL fibres	++	++	+	+
(*c*) day 14				
control	++	+	+	++
pure PVP/PCL fibres	++	+	+	++
PHR-loaded PVP fibres	+++	++	−	+
PHR-loaded PVP/PCL fibres	+++	++	−	−

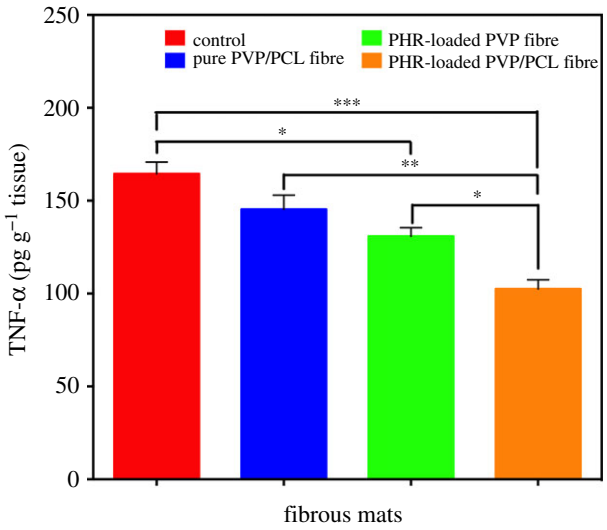

Figure 10. The level of tumour necrosis factor-alpha (TNF-α) in the wounded area of all groups on day 14 after surgical incision. The statistical analyses were carried out with ANOVA test and Bonferroni's *post hoc* test. Values are represented statistically when $*p < 0.05$, $**p < 0.01$, $***p < 0.001$. (Online version in colour.)

($p < 0.05$) and PHR-loaded PVP/PCL fibres ($p < 0.001$) treatment groups compared to control group. Moreover, the decrease of TNF-α level in the PVP/PVL fibres group was statistically more than those in PVP fibres group ($p < 0.05$) and pure fibre group ($p < 0.01$).

Inflammation is the first response by the body when subjected to a skin injury and subsides in less than 5 days [24]. Adequate production of pro-inflammatory mediators is essential to recruit neutrophils and macrophages into the injured site and also to remove bacteria and concomitants from there [25]. However, the sustained expression of these cytokines might lead to more and more inflammatory cell infiltration [24]. Hence, a prolonged inflammatory stage is observed after the end of 5 days, which is known as the late inflammatory phase which might last up to 7 days [26]. In several metabolic diseases such as hyperglycaemia and oxidative stress, this situation is the main responsible factor behind delayed-wound healing [27]. The proliferative and remodelling phases come later and it can be expected that at the end of day 14, wounds are fully covered with neodermis [28].

IL-1β, IL-6 and TNF-α are the primary pro-inflammatory cytokines participating in the migration of immune cells and play a major part in the inflammatory phase. Conversely, IL-10 inhibits pro-inflammatory cytokines and assists wound healing [29]. Previous studies have reported that the expression of TNF-α as well as inflammatory cells was higher in chronic wounds [30,31]. In the present study, the diabetic animals showed a significantly elevated level of TNF-α compared to fibre-treated groups at the end of day 14, which is coherent with the histological findings in that neutrophil infiltration and oedema were still abundant at the same time. Moreover, the PVP/PCL fibre groups had a relatively better healing effect compared to the control group due to long-lasting properties. In addition, TNF-α might prevent the cutaneous step of wound healing through inhibiting the fibroblast actions stimulated by transforming growth factor (TGF-β) and type-1 collagen production [32,33].

Another contribution leading to the prolonged inflammatory phase is considered to be impaired macrophage recruitment. Macrophages are classified into two main groups associated with their metabolism and secretory mediators called M1 and M2. While M1 cells (pro-inflammatory) activate the inflammatory pathways by enhancing the expression of inflammatory mediators such as TNF-α, IL-1 and IL-6, M2 cells (pro-resolution) are capable of alleviating inflammation by producing anti-inflammatory mediators like IL-10 [34–36]. In healthy conditions, there is a balance between the subtypes of macrophages recruited over time, which helps wound healing in a systematic way. In early phases, M1 cells are dominant in the wounded site. As the proliferative phase

emerges, the shift from M1 to M2 macrophages occurs and resolution of inflammation hastens [37]. However, in diabetes, there is a predominance of M1 macrophage type, which encourages the production of inflammatory cytokines and blocks inflammation resolution [26,38].

A PPAR-γ agonist, pioglitazone, binds specific DNA sequences, which in return exhibit intense anti-inflammatory properties either by activating pro-resolving genes, or by inhibiting pro-inflammatory gene transcription or both [39,40]. It has been demonstrated that PPAR-γ activation diminishes the expression of pro-inflammatory proteins and genes including TNF-α [41,42]. Moreover, PPAR-γ activity induces the resolution of inflammation by decreasing M1 cells and increasing M2 cells [38,43,44]. Hence, faster wound healing is achieved. In our study, we observed that both fibre-treated groups showed a better healing process compared to non-treated diabetic animals. It is concluded that these curative effects were provided by anti-inflammatory actions mediated by PPAR-γ activation. It is also shown that our ideas are supported by the decrease of TNF-α levels in fibre-treated animals and PPARγ-mediated M2 macrophage differentiation may accompany anti-inflammatory mechanisms.

On the other hand, TGF-β plays an important role in wound healing by leading to the transition of fibroblasts to myofibroblasts within granulation tissue, enhancing the expression of extracellular matrix components [45]. However, some studies have suggested that when a high level of TGF-β induces the extracellular matrix components, it also impairs the vascularization process [46,47]. Regarding the histological findings in our study, it is concluded that the fibroblast proliferation was higher in both fibre groups than control groups on days 7 and 14. In the light of several previous studies [48,49] showing that PPAR-γ activation increases TGF-β generation, healing effects of fibres may arise from TGF-β induction in fibroblasts.

3.12. Clinical perspectives

In terms of the clinical context of this work, it has the potential to provide a novel and much needed solution to many clinical conundrums. Namely, poor slow-healing chronic ulceration, patient drug compliance, high dosage associated side-effects, poor oral absorption, erratic glycaemic control and therefore a reduction in the morbidity and mortality of diabetes—a condition that has a rising incidence.

Diabetes is a global pandemic affecting 422 million worldwide—quadruple the number since 1980. The cost of diabetes to the UK National Health Service is over £1.5 million an hour, which equates to over £25 000 being spent on diabetes every minute and an annual estimated spend of £14 billion, with the cost of treating complications representing a much higher cost. It has micro- and macrovascular complications that can have a devastating impact on patient quality of life, ranging from fulminant renal failure requiring dialysis to blindness in the extreme. Diabetes-related foot complications have been identified as the single most common cause of morbidity among diabetic patients. Diabetic foot ulcers are a common complication of long-term diabetes, with around 20% of people with diabetes developing them. Foot ulcers can lead to lengthy hospital stays and potentially amputations. The complicating factor of underlying peripheral vascular disease renders the majority of diabetic foot ulcers asymptomatic until the progression to non-healing ulcers. Therefore, aggressive and novel treatment strategies are critical.

The key to its successful treatment is, therefore, tight control of blood glucose and promotion of the healing process. Pioglitazone is a widely used existing oral drug treatment and has an absolute bioavailability of 83%. Its mechanism of action is as a PPAR-γ agonist; it increases transcription of insulin-responsive genes. It increases insulin sensitivity in target tissues and decreases hepatic gluconeogenesis. It does, however, have a significant side effect profile via oral administration including exacerbation of heart failure, increased risk of fractures, higher risk of bladder cancer and hypoglycaemia. The use of pioglitazone in this capacity offers higher bioavailability, targeted entry to the wound site and reduced systemic side effects. The prospect of sustained release treatment could mean reduced frequency of medication needed as well.

Wound closure by primary intention involves key stages: haemostasis, inflammation, proliferation and remodelling. Timing is critically important to wound healing. Most significantly, the timing of wound re-epithelialization can decide the outcome of the healing. This mechanism is dysregulated in a diabetic patient. However, this research has shown that treatment with PHR-loaded fibrous mats decreased neutrophil infiltration, oedema, and inflammation and increased epidermal regeneration and fibroblast proliferation. These findings are supported by other research that PPAR-γ modulates the immune response and expression of inflammatory cytokines in the healing process.

Ideal treatments share many qualities found in these fibrous mats. For example, the biodegradability and bioavailability of the PCL and the PG technique and its capacity for mass production [10]. The lack of cytotoxic effects also is encouraging. Most notably is the faster healing promotion. This research has extensively tested the theories hypothesized on both a histopathological and biochemical level on animal subjects. The promise of targeted treatment on the wound surface as routine and mass market application of diabetic ulcers is an exciting one and further research is needed to translate this vision to humans.

4. Conclusions

In this study, biodegradable PHR-loaded fibrous mats with two different release kinetics were successfully fabricated and compared for their efficiency in diabetic wound healing with *in vitro* and *in vivo* tests. It was clearly shown that PHR-loaded fibrous mats accelerated diabetic wound healing with no cytotoxicity, albeit with different release kinetics and efficacies but the sustained release was significantly more effective according to histological and biochemical evaluations. Treatment with PHR-loaded fibrous mats decreased neutrophil infiltration, oedema, and inflammation and increased epidermal regeneration and fibroblast proliferation compared to pure fibre but the formation of hair follicles and completely improved oedema were observed only in the sustained release form. Besides, the tensile strength of the PVP/PCL fibrous mats was superior than that of PVP only. Moreover, the effectiveness of sustained release in this study was again established. One of the most important key points is the production of fibres by the PG technique, which is a suitable technique for mass production. The experimental results herein suggest that topical administration of sustained released PPAR-γ agonist inside fibrous mats has high potential for the treatment of diabetic wounds especially during the

inflammatory and proliferative phases of healing with high bioavailability and fewer systemic side effects.

Ethics. All animal experiments were carried out at Marmara University with the approval of the Marmara University Animal Experiments Local Ethics Committee (MUHDEK) (permission number: 114.2018mar).

Data accessibility. The datasets supporting this article have been uploaded as part of the electronic supplementary material.

Authors' contributions. M.E.C., H.A. and M.E. drafted and revised the manuscript, designed the study and produced the fibrous mats. M.E.C. and S.Y. performed animal experiments and biochemical analysis. S.C. and O.G. characterized the fibrous mats. G.S.O. and D.A. performed histological analysis. G.E. and D.S.K. performed the MTT test. U.E. drafted the manuscript and made a clinical overview. L.K. performed data analysis. All authors proofread the manuscript and approved the final version.

Competing interests. The authors have no competing interests.

Funding. H.A. wishes to thank PAAET-Kuwait for sponsoring his doctoral research at UCL (grant no. 278010301647).

Acknowledgements. M.E.C. was supported by a TUBITAK 2219 Research Programme Grant (Scientific and Technological Research Council of Turkey-TUBITAK) and thanks UCL Mechanical Engineering for hosting his post-doctoral research in the UK.

References

1. Cam ME, Hazar-Yavuz AN, Yildiz S, Ertas B, Ayaz Adakul B, Taskin T, Alan S, Kabasakal L. 2019 The methanolic extract of *Thymus praecox* subsp. skorpilii var. skorpilii restores glucose homeostasis, ameliorates insulin resistance and improves pancreatic β-cell function on streptozotocin/nicotinamide-induced type 2 diabetic rats. *J. Ethnopharmacol.* **231**, 29–38. (doi:10.1016/j.jep.2018.10.028)
2. Han G, Ceilley R. 2017 Chronic wound healing: a review of current management and treatments. *Adv. Ther.* **34**, 599–610. (doi:10.1007/s12325-017-0478-y)
3. Cam ME, Cesur S, Taskin T, Erdemir G, Kuruca DS, Sahin YM, Kabasakal L, Gunduz O. 2019 Fabrication, characterization and fibroblast proliferative activity of electrospun *Achillea lycaonica*-loaded nanofibrous mats. *Eur. Polym. J.* **120**, 109239. (doi:10.1016/j.eurpolymj.2019.109239)
4. Huang X, Brazel CS. 2001 On the importance and mechanisms of burst release in matrix-controlled drug delivery systems. *J. Control. Release* **73**, 121–136. (doi:10.1016/S0168-3659(01)00248-6)
5. Wang L, Chang M-W, Ahmad Z, Zheng H, Li J-S. 2017 Mass and controlled fabrication of aligned PVP fibers for matrix type antibiotic drug delivery systems. *Chem. Eng. J.* **307**, 661–669. (doi:10.1016/j.cej.2016.08.135)
6. Setterstrom JA, Tice TR, Myers WE. 1984 Development of encapsulated antibiotics for topical administration to wounds. In *Recent advances in drug delivery systems* (eds JM Anderson, SW Kim), pp. 185–198. Boston, MA: Springer. (doi:10.1007/978-1-4613-2745-5_12)
7. Kim GM, Le KH, Giannitelli SM, Lee YJ, Rainer A, Trombetta M. 2013 Electrospinning of PCL/PVP blends for tissue engineering scaffolds. *J. Mater. Sci. Mater. Med.* **24**, 1425–1442. (doi:10.1007/s10856-013-4893-6)
8. Wang JC, Zheng H, Chang MW, Ahmad Z, Li JS. 2017 Preparation of active 3D film patches via aligned fiber electrohydrodynamic (EHD) printing. *Sci. Rep.* **7**, 43924. (doi:10.1038/srep43924)
9. Alenezi H, Cam ME, Edirisinghe M. 2019 Experimental and theoretical investigation of the fluid behavior during polymeric fiber formation with and without pressure. *Appl. Phys. Rev.* **6**, 041401. (doi:10.1063/1.5110965)
10. Heseltine PL, Ahmed J, Edirisinghe M. 2018 Developments in pressurized gyration for the mass production of polymeric fibers. *Macromol. Mater. Eng.* **303**, 1800218. (doi:10.1002/mame.201800218)
11. Tan NS, Michalik L, Noy N, Yasmin R, Pacot C, Heim M, Flühmann B, Desvergne B, Wahli W. 2001 Critical roles of PPAR β/δ in keratinocyte response to inflammation. *Genes Dev.* **15**, 3263–3277. (doi:10.1101/gad.207501)
12. Tyagi S, Gupta P, Saini AS, Kaushal C, Sharma S. 2011 The peroxisome proliferator-activated receptor: a family of nuclear receptors role in various diseases. *J. Adv. Pharm. Technol. Res.* **2**, 236–240. (doi:10.4103/2231-4040.90879)
13. Chen H *et al.* 2015 Macrophage peroxisome proliferator-activated receptor γ deficiency delays skin wound healing through impairing apoptotic cell clearance in mice. *Cell Death Dis.* **6**, e1597. (doi:10.1038/cddis.2014.544)
14. Ahmed J, Matharu RK, Shams T, Illangakoon UE, Edirisinghe M. 2018 A comparison of electric-field-driven and pressure-driven fiber generation methods for drug delivery. *Macromol. Mater. Eng.* **303**, 1700577. (doi:10.1002/mame.201700577)
15. Brako F, Raimi-Abraham BT, Mahalingam S, Craig DQM, Edirisinghe M. 2018 The development of progesterone-loaded nanofibers using pressurized gyration: a novel approach to vaginal delivery for the prevention of pre-term birth. *Int. J. Pharm.* **540**, 31–39. (doi:10.1016/j.ijpharm.2018.01.043)
16. Xue J, Wu T, Dai Y, Xia Y. 2019 Electrospinning and electrospun nanofibers: methods, materials, and applications. *Chem. Rev.* **119**, 5298–5415. (doi: 10.1021/acs.chemrev.8b00593)
17. Pandit V, Pai R, Devi K, Suresh S. 2012 *In vitro–in vivo* evaluation of fast-dissolving tablets containing solid dispersion of pioglitazone hydrochloride. *J. Adv. Pharm. Technol. Res.* **3**, 160–170. (doi:10.4103/2231-4040.101008)
18. Chowdary DY, Raparla R, Madhuri M. 2014 Formulation and evaluation of multilayered tablets of pioglitazone hydrochloride and metformin hydrochloride. *J. Pharm. (Cairo)* **2014**, 848243. (doi:10.1155/2014/848243)
19. Qian X-F, Yin J, Feng S, Liu S-H, Zhu Z-K. 2001 Preparation and characterization of polyvinylpyrrolidone films containing silver sulfide nanoparticles. *J. Mater. Chem.* **11**, 2504–2506. (doi:10.1039/B103708K)
20. Hemanth A, Anand Kumar Y. 2016 Preparation and evaluation of pioglitazone HCl solid dispersions. *J. Chronother. Drug Deliv.* **7**, 73–82.
21. Qian Y, Zhang Z, Zheng L, Song R, Zhao Y. 2014 Fabrication and characterization of electrospun polycaprolactone blended with chitosan–gelatin complex nanofibrous mats. *J. Nanomater.* **2014**, 964621. (doi:10.1155/2014/964621)
22. Jain SK, Jain A, Gupta Y, Kharya A. 2008 Design and development of a mucoadhesive buccal film bearing progesterone. *Pharmazie* **63**, 129–135. (doi:10.1691/ph.2008.7114)
23. Leask A. 2013 The contribution of peroxisome proliferator-activated receptor gamma to cutaneous wound healing. *Adv. Wound Care* **2**, 69–73. (doi:10.1089/wound.2012.0362)
24. Zhang XN, Ma ZJ, Wang Y, Li YZ, Sun B, Guo X, Pan CQ, Chen LM. 2016 The four-herb Chinese medicine formula Tuo-Li-Xiao-Du-San accelerates cutaneous wound healing in streptozotocin-induced diabetic rats through reducing inflammation and increasing angiogenesis. *J. Diabetes Res.* **2016**, 5639129. (doi:10.1155/2016/5639129)
25. Tan WS, Arulselvan P, Ng SF, Mat Taib CN, Sarian MN, Fakurazi S. 2019 Improvement of diabetic wound healing by topical application of Vicenin-2 hydrocolloid film on Sprague Dawley rats. *BMC Complement. Altern. Med.* **19**, 20. (doi:10.1186/s12906-018-2427-y)
26. Rodrigues HG *et al.* 2016 Oral administration of linoleic acid induces new vessel formation and improves skin wound healing in diabetic rats. *PLoS ONE* **11**, e0165115. (doi:10.1371/journal.pone.0165115)
27. Thangavel P, Kannan R, Ramachandran B, Moorthy G, Suguna L, Muthuvijayan V. 2018 Development of reduced graphene oxide (rGO)-isabgol nanocomposite dressings for enhanced vascularization and accelerated wound healing in normal and diabetic rats. *J. Colloid Interface Sci.* **517**, 251–264. (doi:10.1016/j.jcis.2018.01.110)
28. He M, Sun L, Fu X, McDonough SP, Chu CC. 2019 Biodegradable amino acid-based poly(ester amine) with tunable immunomodulating properties and their *in vitro* and *in vivo* wound healing studies in diabetic rats' wounds. *Acta Biomater.* **84**, 114–132. (doi:10.1016/j.actbio.2018.11.053)

29. de Aragao Tavares E *et al.* 2018 Chitosan membrane modified with a new zinc(II)-vanillin complex improves skin wound healing in diabetic rats. *Front. Pharmacol.* **9**, 1511. (doi:10.3389/fphar.2018.01511)
30. Zhang Q, Oh JH, Park CH, Baek JH, Ryoo HM, Woo KM. 2017 Effects of dimethyloxalylglycine-embedded poly(epsilon-caprolactone) fiber meshes on wound healing in diabetic rats. *ACS Appl. Mater. Interfaces* **9**, 7950–7963. (doi:10.1021/acsami.6b15815)
31. Qiu Z, Kwon AH, Kamiyama Y. 2007 Effects of plasma fibronectin on the healing of full-thickness skin wounds in streptozotocin-induced diabetic rats. *J. Surg. Res.* **138**, 64–70. (doi:10.1016/j.jss.2006.06.034)
32. Lai JJ, Lai KP, Chuang KH, Chang P, Yu IC, Lin WJ, Chang C. 2009 Monocyte/macrophage androgen receptor suppresses cutaneous wound healing in mice by enhancing local TNF-α expression. *J. Clin. Invest.* **119**, 3739–3751. (doi:10.1172/jci39335)
33. Goldberg MT, Han YP, Yan C, Shaw MC, Garner WL. 2007 TNF-alpha suppresses alpha-smooth muscle actin expression in human dermal fibroblasts: an implication for abnormal wound healing. *J. Invest. Dermatol.* **127**, 2645–2655. (doi:10.1038/sj.jid.5700890)
34. Mirza RE, Fang MM, Weinheimer-Haus EM, Ennis WJ, Koh TJ. 2014 Sustained inflammasome activity in macrophages impairs wound healing in type 2 diabetic humans and mice. *Diabetes* **63**, 1103–1114. (doi:10.2337/db13-0927)
35. Rodrigues HG *et al.* 2017 Correction: oral administration of linoleic acid induces new vessel formation and improves skin wound healing in diabetic rats. *PLoS ONE* **12**, e0179071. (doi:10.1371/journal.pone.0179071)
36. Yu T, Gao M, Yang P, Liu D, Wang D, Song F, Zhang X, Liu Y. 2019 Insulin promotes macrophage phenotype transition through PI3 K/Akt and PPAR-gamma signaling during diabetic wound healing. *J. Cell. Physiol.* **234**, 4217–4231. (doi:10.1002/jcp.27185)
37. Shook B, Xiao E, Kumamoto Y, Iwasaki A, Horsley V. 2016 CD301b+ macrophages are essential for effective skin wound healing. *J. Invest. Dermatol.* **136**, 1885–1891. (doi:10.1016/j.jid.2016.05.107)
38. Mirza RE, Fang MM, Novak ML, Urao N, Sui A, Ennis WJ, Koh TJ. 2015 Macrophage PPARγ and impaired wound healing in type 2 diabetes. *J. Pathol.* **236**, 433–444. (doi:10.1002/path.4548)
39. Chawla A. 2010 Control of macrophage activation and function by PPARs. *Circ. Res.* **106**, 1559–1569. (doi:10.1161/circresaha.110.216523)
40. Straus DS, Glass CK. 2007 Anti-inflammatory actions of PPAR ligands: new insights on cellular and molecular mechanisms. *Trends Immunol.* **28**, 551–558. (doi:10.1016/j.it.2007.09.003)
41. Elshazly S, Soliman E. 2019 PPAR gamma agonist, pioglitazone, rescues liver damage induced by renal ischemia/reperfusion injury. *Toxicol. Appl. Pharmacol.* **362**, 86–94. (doi:10.1016/j.taap.2018.10.022)
42. Refaie MMM, El-Hussieny M. 2018 Protective effect of pioglitazone on ovarian ischemia reperfusion injury of female rats via modulation of peroxisome proliferator activated receptor gamma and heme-oxygenase 1. *Int. Immunopharmacol.* **62**, 7–14. (doi:10.1016/j.intimp.2018.06.037)
43. Sakai S, Sato K, Tabata Y, Kishi K. 2016 Local release of pioglitazone (a peroxisome proliferator-activated receptor gamma agonist) accelerates proliferation and remodeling phases of wound healing. *Wound Repair Regen.* **24**, 57–64. (doi:10.1111/wrr.12376)
44. Spencer M, Yang L, Adu A, Finlin BS, Zhu B, Shipp LR, Rasouli N, Peterson CA, Kern PA. 2014 Pioglitazone treatment reduces adipose tissue inflammation through reduction of mast cell and macrophage number and by improving vascularity. *PLoS ONE* **9**, e102190. (doi:10.1371/journal.pone.0102190)
45. Barrientos S, Stojadinovic O, Golinko MS, Brem H, Tomic-Canic M. 2008 Growth factors and cytokines in wound healing. *Wound Repair Regen.* **16**, 585–601. (doi:10.1111/j.1524-475X.2008.00410.x)
46. Geng L, Chaudhuri A, Talmon G, Wisecarver JL, Wang J. 2013 TGF-Beta suppresses VEGFA-mediated angiogenesis in colon cancer metastasis. *PLoS ONE* **8**, e59918. (doi:10.1371/journal.pone.0059918)
47. Costa PZ, Soares R. 2013 Neovascularization in diabetes and its complications. Unraveling the angiogenic paradox. *Life Sci.* **92**, 1037–1045. (doi:10.1016/j.lfs.2013.04.001)
48. Liao H, Pastar I, Chen W. 2012 Rosiglitazone modulates the behaviors of diabetic host-derived fibroblasts in a carboxymethyllysine-modified collagen model. *Wound Repair Regen.* **20**, 435–443. (doi:10.1111/j.1524-475X.2012.00795.x)
49. Wang H, Ye P, Li Y, Li ZB, Wang L. 2013 Effects of pioglitazone on TGFbeta1 expression in ischemia/reperfusion injury myocardium of rats. *Chinese J. Appl. Physiol.* **29**, 1–4.